HF RFID Tag Location Using Magneto-inductive waves

Richard. R.A. Syms, *Senior Member IEEE*, Artem Voronov, and Oleksiy Sydoruk

***Abstract*— Location of passive RFID tags in the HF regime presents significant problems, because of the absence of radiating fields at the low frequencies involved. Here we present a solution for one-dimensional localization based on magneto-inductive (MI) waves. Passive tags are interrogated using a travelling wave antenna based on a MI waveguide, a magnetically coupled array of $L-C$ resonators supporting travelling waves. Load modulation signals generated by the tag during its unique identifier response are coupled into the waveguide and travel to either end with low group velocity. Signal timings are measured by cross-correlation, and the tag position is estimated to the nearest resonant loop from the difference in their arrival times. Correlation detection is demonstrated using a system model, and theoretical predictions are confirmed using an experimental system containing eleven transformer-coupled resonators operating at 13.56 MHz frequency. Accurate localization is obtained up to the tag reading limit using <1W RF power.**

***Index Terms*— Magneto-inductive waveguide, near-field communication, RFID, travelling wave antenna.**

I. Introduction

RADIO-FREQUENCY identification (RFID) is a method of asset identification, also applied to tickets, smart cards and smart wallets [1], [2]. Communication takes place between a single reader and a tag, which is itself powered by the reader [3]. In the high frequency (HF) regime, the reader and tag antennas are resonant inductive loops, and communication is in the near field, often based on the ISO/IEC 14443 standard [4]. Powering and communication both have poor range scaling [5]. The lack of phase information limits algorithms to exploitation of relative signal strength (RSS) and prevents accurate range- and direction-finding. Despite this, antennas with improved spatial selectivity [6]-[9] and antenna arrays [10, 11] have both been developed. HF RFID tag location has been used for inventory management [12], [13], and tag arrays have been used for navigation [14]-[19]. In each case, systems operate by detection of the nearest tag using a single moving reader and ranges are limited to a few cm. UHF RFID has seen a proliferation of localization schemes based on signal strength or phase derived from single or multiple tags and acquired by single or multiple readers, for example as summarized in Table I [20]-[27]. Reviews can be found in [28]-[30]. In contrast, HF RFID tracking methods are relatively undeveloped.

TABLE I
METHODS OF UHF RFID LOCALIZATION

Located object	Reference system	Method	Reference
Reader	Multiple fixed tags	Signal strength	20, 22
Reader	Multiple fixed tags	Signal phase	24
Tag	Multiple fixed antennas	Signal phase	21, 23, 27
Tag	Single moving antenna	Signal strength	25
Tag	Single moving antenna	Signal phase	26

One solution to HF RFID localization may be conversion to a non-radiative travelling wave, such as a magneto-inductive (MI) wave, a slow wave that propagates in arrays of magnetically coupled resonant loops [31]-[33]. Low-loss flexible MI cables [34] and broadband coupling transducers [35] have both been developed. MI waves have been used for communication [36]-[38] and load position sensing [39]-[42], and a HF RFID receiver based on a MI antenna has been demonstrated [43]. The aim of this paper is to explore the use of MI waves for tag location, to enable asset or user tracking in one dimension. As in radar and sonar, position is estimated from time-of-flight (TOF) measurement. Key differences are that the signals are emitted by the tags, at unknown times, and vary from tag-to-tag. Despite this, we show that correlation detection [44] can allow localization based on the TOF difference between signals detected at either end of a MI antenna during the unique identifier (UID) response.

Fig. 1 shows a block diagram of the proposed system. The antenna is a magneto-inductive waveguide, a linear array of magnetically coupled $L-C$ resonators [31]-[33]. The transmit (TX) signal from the reader is coupled into the antenna at one end using a frequency-selective filter coupler tuned to the carrier frequency, and a similar coupler is used to transfer

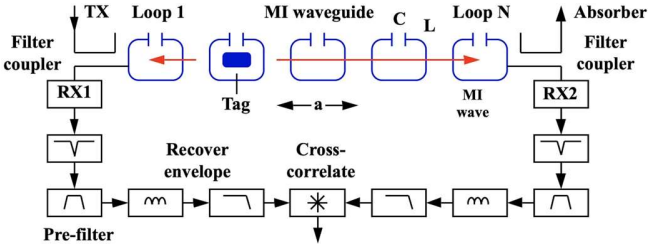

Fig. 1. System block diagram for tag localization by cross-correlation of magneto-inductive waves.

Manuscript received Month xx, 2xxx; revised Month xx, xxxx; accepted Month x, xxxx.

The authors are with the Department of Electrical and Electronic Engineering, Imperial College London, London, SW7 2AZ, U.K. (e-mail: r.syms@imperial.ac.uk; artem.voronov14@imperial.ac.uk; o.sydoruk@imperial.ac.uk).

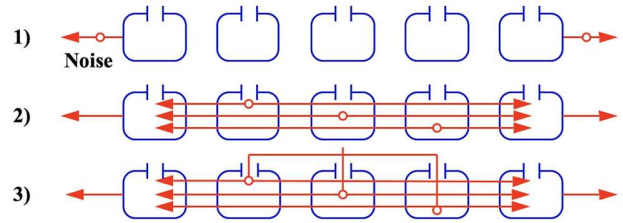

Fig. 2. Noise sources in a MI waveguide: 1) uncorrelated, 2) weakly correlated and 3) strongly correlated.

residual carrier to an absorber at the other. TX signals power the tag, which acts as a localized load that may in principle be used for position sensing [40]-[42]. When interrogated, the tag uses a subcarrier to induce a time-varying load in an antenna element, which results in reflected and transmitted slow waves at carrier sideband frequencies. Such signals can be extracted from either end of the antenna. In the absence of loss, the signals are position-independent, so the antenna can be axially extended to increase capture volume without detriment to efficiency [43]. High antenna bandwidth removes the need to artificially load resonators, and losses can be kept low by maximizing element Q-factors. The sidebands are separated from the carrier using the filter couplers and detected by two receivers (RX1 and RX2). Software notch and bandpass pre-filters are used to suppress residual carrier and out-of-band noise [44]. Envelopes are recovered, UIDs are decoded, the signals are correlated together [45], and position is determined from the TOF difference Δt of the two signals thus obtained.

The use of a slow-wave structure reduces demands on electronics. However, limits to localization must be set by dispersion, which reduces the intrinsic similarity of the two signals. Performance must also depend on the signal-to-noise ratio (SNR) and the nature of the noise. Fig. 2 shows three possible noise sources, which include 1) uncorrelated receiver noise, 2) partly correlated noise from the antenna itself and 3) ambient RF noise detected by the antenna. Obvious sources of internal noise are thermal and shot noise. External noise sources include switches, motors, vehicle ignition, plasma processing [46] and, increasingly, computers [47]. External noise must generate strongly correlated outputs, which may lead to a false correlation at $\Delta t = 0$.

These limitations will be explored in the following sections. The design of MI antennas is reviewed in Section 2, and the method of time-of-flight estimation is introduced. The autocorrelation properties of UID responses (which must vary from tag to tag) are studied in Section 3. Simulations based on an approximate system model are presented in Section 4. Predictions are verified experimentally in Section 5 using a custom reader and a small-scale MI antenna with an overall length of $\sim 2m$. Conclusions are drawn in Section 6.

II. Antenna Design

In this section we consider the properties of an MI antenna, one example of an extended structure capable of creating and detecting magnetic fields suitable for HF RFID.

Each loop in Fig. 1 is assumed to have inductance L (with associated resistance R) and capacitance C, and be coupled to its nearest neighbors by mutual inductance M. In the absence of voltage sources, the circuit equation relating the current I_n in element n to the currents in elements $n-1$ and $n+1$ and at angular frequency ω is:

$$\left(R + j\omega L + \frac{1}{j\omega C}\right) I_n + j\omega M(I_{n-1} + I_{n+1}) = 0. \quad (1)$$

Assumption of travelling wave solutions in the form $I_n = I_0 \exp(-jnka)$, where I_0 is the current amplitude, k is the propagation constant and a is the element spacing, leads to the dispersion equation [32]:

$$1 - \frac{\omega_0^2}{\omega^2} - j\frac{\omega_0}{\omega Q} + \kappa\cos(ka) = 0. \quad (2)$$

Here $\omega_0 = 1/\sqrt{LC}$ is the angular resonant frequency, $\kappa = 2M/L$ is the coupling coefficient and $Q = \omega_0 L/R$ is the quality factor. In the absence of losses, k is real in band, and may be positive or negative depending on the sign of the mutual inductance M. Propagation is then band-limited to the range:

$$\frac{1}{\sqrt{1+|\kappa|}} \le \frac{\omega}{\omega_0} \le \frac{1}{\sqrt{1-|\kappa|}}. \quad (3)$$

The effect of loss (when R is non-zero and Q is finite) is to render the propagation constant complex, so that $k = k' - jk''$. Waves are then attenuated, and out-of-band propagation arises.

The bandwidth should be sufficient to allow propagation of the whole ISO/IEC 14443 spectrum. For example, Fig. 3 shows the variations of $k'a$ and $k''a$ with frequency for a waveguide with $f_0 = \omega_0/2\pi = 13.56\,MHz$, $\kappa = -0.50$ and $Q = 200$, chosen for comparison with later experiments. Here the portion of the dispersion diagram showing positive group velocity has been plotted. The slope of the dispersion characteristic (upper diagram) is close to zero near the band edges when $k'a = 0$ or π, and rises to a maximum within the band. The value of $k''a$ (lower diagram) is low within the propagating band but rises rapidly outside it. For high Q-factors, propagation losses are minimised at f_0. The dotted lines, which show the two sub-carrier frequencies, indicate the approximate bandwidth needed. This guide is suitable but guides with lower values of $|\kappa|$ may not be.

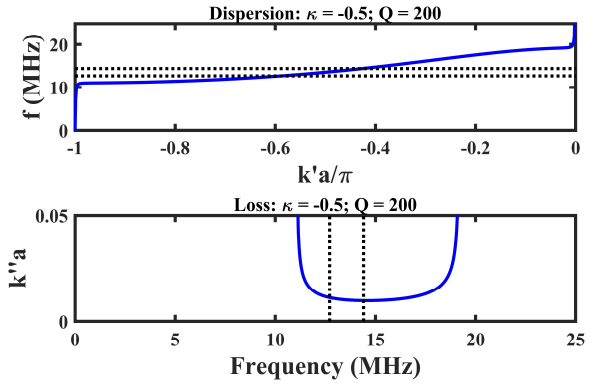

Fig. 3. Theoretical variations of $k'a$ (upper diagram) and $k''a$ (lower) with frequency for a MI waveguide with $f_0 = 13.56\,MHz$, $\kappa = -0.5$ and $Q = 200$.

For lossless systems, the characteristic impedance is [33]:

$$Z_0 = j\omega M \exp(-jka) \quad (4)$$

Generally, the characteristic impedance is complex;

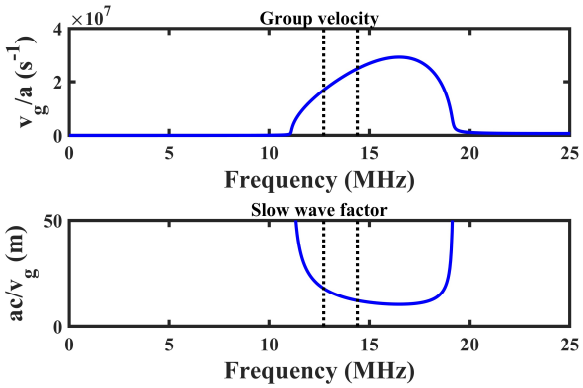

Fig. 4. Theoretical variations of v_g/a (upper diagram) and ac/v_g (lower) with frequency for a MI waveguide with $f_0 = 13.56\ MHz$, $\kappa = -0.5$ and $Q = 200$.

however, at resonance, it reduces to the real value $Z_{0M} = \omega_0|M|$, allowing matching to conventional systems. Improved matching may be obtained using terminating elements with inductance $L/2$ and capacitance $2C$ [35]. Full system simulations may be carried out by solving circuit equations of the type in (1) or by constructing transfer functions.

Differentiating the lossless dispersion equation, the group velocity $v_g = d\omega/dk$ of MI waves may be found as [42]:

$$v_g = \frac{\kappa a \sin(ka)\omega^3}{2\omega_0^2} \tag{5}$$

The upper diagram in Fig. 4 shows variations of v_g/a with frequency, for the same parameters. The group velocity rises from zero at the band edges to a maximum at intermediate frequency. For small $|\kappa|$, this maximum is located at ω_0; however, it shifts to higher frequency as $|\kappa|$ increases. The slow wave factor SWF can be found by comparing v_g with the velocity c of an electromagnetic wave in free space. The lower diagram in Fig. 4 shows the variation of ac/v_g with frequency. The group velocity at resonance is $v_{g0} = |\kappa|a\omega_0/2$. For the previous parameters we then obtain, $ac/v_{g0} = 2c/= |\kappa|\omega_0 \approx 15$. For $a = 15cm$, say, we then obtain $SWF = 100$, a relatively large value that improves timing accuracy. For $a = 1.5m$, the slow wave factor reduces to 10.

The TOF differences Δt that must be measured to detect distance-of-flight (DOF) differences Δx have the form $\Delta t = \Delta x/v_g$. Since the tag can only be displaced from the waveguide center by a whole number of loops, $\Delta x = 2\nu a$, where ν is integer. At resonance, $\Delta t = 4\nu/|\kappa|\omega_0$. In terms of the period $T = 2\pi/\omega_0$, we obtain $\Delta t/T = 2\nu/|\kappa|\pi$. For $\kappa = -0.50$, the minimum TOF difference that must be detected is then $\Delta t/T \approx 4/\pi \approx 1.273$. To reduce timing errors below 10%, sampling must be carried out at a frequency $f_s > 12.73 f_0$, or at least $173\ MSa/s$. However, reduced accuracy may be sufficient.

With low signal distortion, it should then be possible to estimate values of Δt using correlation detection. However, because of the wide signal bandwith, localization accuracy will be degraded by envelope changes. The group velocity dispersion $GVD = d(1/v_g)/d\omega$ is:

$$GVD = \frac{-2\omega_0^2}{\kappa a \omega^4 \sin(ka)}\left\{3 + \frac{2\omega_0^2 \cos(ka)}{\kappa\omega^2 \sin^2(ka)}\right\} \tag{6}$$

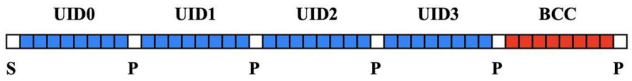

Fig. 5. Construction of binary tag UID response.

The GVD is zero when the contents of the curly bracket above vanish, allowing the frequency of zero dispersion ω_Z to be found as:

$$\frac{\omega_Z}{\omega_0} = \frac{1}{\sqrt{2 - \sqrt{1 + 3\kappa^2}}} \tag{7}$$

This ratio is unity when $|\kappa|$ is low, but gradually rises as $|\kappa|$ increases. Our studies have shown that operation at ω_Z rather than ω_0 allows some reduction in envelope distortion, but at a price of higher losses; consequently, there is little obvious advantage in operating away from resonance.

III. TAG RESPONSES

In this section, we consider the correlation properties of tag responses defined by ISO/IEC 14443, a common standard for proximity-coupled cards that uses the unlicensed industrial, scientific, and medical (ISM) band at f_0 = 13.56 MHz [4]. Attention is focused on the UID response since this must be recovered in any reader. Tag position is assumed to be found by correlation due to the large processing gain available.

For Type A transponders, reader queries are transmitted in modified Miller code on sub-carriers separated by $f_0 = 13.56\ MHz$ from the carrier using close to 100% amplitude shift key (ASK) at $f_0/128 = 106\ kB/s$. Tags respond using Manchester code with on-off key (OOK) sub-carrier load modulation. Although this protocol was not designed for tag location, autocorrelation envelopes suitable for timing can be obtained from 4-byte Type A UID responses, as we now show. Fig. 5 shows the binary equivalent of the tag responses. The response begins with a start bit S. Each UID byte is followed by a separate parity bit P, and the last byte is followed by a block check code BCC, obtained as a bitwise exclusive OR of the four UID bytes and again followed by a parity bit. The binary response is Manchester-coded with a 'one' as a 1-0 transition and a 'zero' as a 0-1 transition, doubling the bandwidth. The binary response then contains 1 + 5 x 9 = 46 bits, and the Manchester coded response contains 92 chips.

Performance of such responses in a correlation detection system may be estimated as follows. The processing gain G may be estimated as the bandwidth expansion factor, namely $92N_S$, where N_S is the number of samples per chip. If N_S is only moderate, the processing gain can be large (for example, $G > 2000$ for N_S =48). Because half of the chips are zero, the peak of each autocorrelation is $46N_S$ times the signal strength. Correlation detection is therefore an intrinsically low noise operation.

In contrast to radar responses, UID autocorrelations are not ideal delta functions. Ability to locate the correlation peak then depends on the sidelobe ratio (SLR). Its value may be estimated by assuming a two-chip offset for binary codes consisting entirely of 'ones' as $SLR = 46/45 = 1.0222$. However, the BCC byte prevents this case arising in practice. For example, Fig. 6a shows the baseband response and ideal autocorrelation

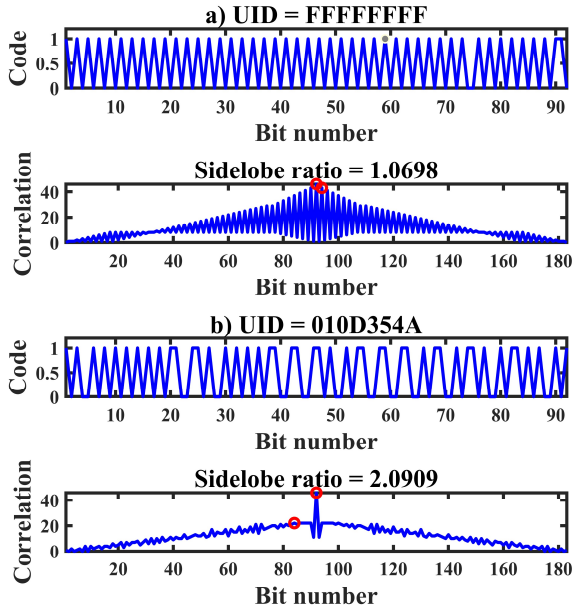

Fig. 6. Baseband Manchester coded UID responses (upper diagrams) and their autocorrelations (lower), for UIDs with a) low and b) high sidelobe ratios.

of $UID = FFFFFFFF$, where BCC has introduced discontinuities in the otherwise regular code. These have increased the sidelobe ratio to 46/43 = 1.0698. Despite this, the envelope of the autocorrelation function is still broad.

The UID above is the worst case we have identified. Using a numerical search of one eighth of all possible UIDs (which number 256^4 = 4.29 x 10^9), we have found that SLR does not fall below 1.0698, and that the autocorrelation peak sharpens as the code becomes more random, with a maximum $SLR = 46/22 = 2.0909$. In this case, the autocorrelation consists of a sharp peak generated by the code itself, superimposed on a triangular base arising from its average level. For example, Fig. 6b shows the baseband response and autocorrelation for $UID = 010D354A$, which has the peak SLR found. Similar autocorrelations are common, allowing timing by location of the sharp central peak, whose shape is largely determined by the autocorrelation of a single bit.

IV. System Simulation

In this section, we describe a simulation of the system in Fig. 1, carried out in Matlab®. Tag loading effects are ignored, and the frequency variation of the propagation constant is first found by solving the MI dispersion equation for a uniform waveguide with $f_0 = 13.56\,MHz$ and given κ and Q. For any tag position P, this variation is used to calculate transfer functions for the two counter-propagating waves, in the form $T_1 = \exp(-jN_1ka)$ and $T_2 = \exp(-jN_2ka)$, where $N_1 = P - 1$ and $N_2 = N - P$. The effect of the filter couplers is ignored since it is similar to the notch filters. Transfer functions T_{FN} and T_{FB} for the notch and bandpass filters are also calculated. Here notch filters were used to achieve 60 dB carrier suppression with minimal sideband attenuation, while high-order Butterworth filters were used to reject out-of-band noise. A small trade-off between dispersion- and noise-induced errors obtained by adjusting their bandwidth was noted.

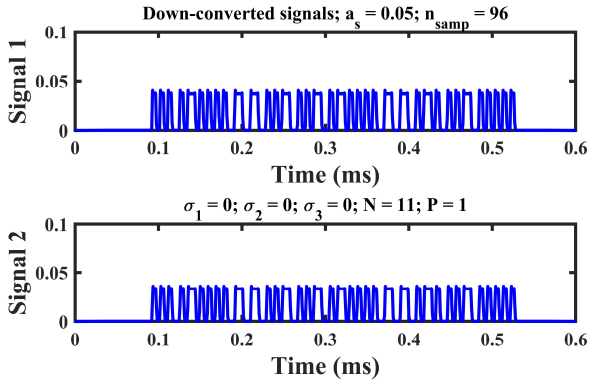

Fig. 7. Simulated noiseless signals after filtering and down-conversion for $UID = F38FEA95$, assuming $N = 11$ and $P = 1$, assuming carrier and modulation amplitudes of 1.0 and 0.05.

The baseband Manchester code equivalent s_T of a given UID is first constructed and used to modulate at the subharmonic frequency a vector representing a carrier sampled at $f_s = 96f_0$. The resulting vector s_0 is used to represent the load-modulation signal. Propagation and filtering are simulated by using the discrete Fourier transform to obtain the frequency domain equivalent S_0, multiplying by the transfer functions of the MI waveguide (T_1 or T_2) and filters (T_{FN} and T_{FB}), and using the inverse Fourier transform to generate time domain signals s_1 and s_2. A Tukey window is used to remove artifacts at window edges. Baseband envelopes are extracted by rectification and convolution with a rectangular window. Envelopes are converted to binary by correlation with Manchester transitions and UIDs are recovered after checking parity and BCC. s_1 and s_2 are cross-correlated, and Δt is found from the difference in peak times obtained from each correlation order. The tag position P_{est} is estimated using the group velocity v_g, and correct localisation is assumed if the position error $\Delta P = P_{est} - P$ satisfies $|\Delta P| < 0.5$.

The following results show noiseless simulations of an 11-element MI waveguide with $\kappa = -0.5$ and $Q = 200$, assuming carrier and modulation amplitudes of 1 and 0.05. A tag with $UID = F38FEA95$ is assumed to be at $P = 1$. Fig. 7 shows simulated signals s_1 and s_2 after filtering and down-conversion, both clearly representing binary codes.

Fig. 8 shows the result of processing these signals to check parity (here, both pass) and BCC ('PP' = both pass) and extract the UIDs (both are correct), together with the two possible correlations. The complete variation (upper plot) shows that the correlation envelopes are extremely similar. However, expansion of the peak over a shorter timescale (lower plot) shows a small time-difference, which can be used to estimate the tag position. The error ΔP is clearly low. Its cause is group velocity dispersion, which has rounded the correlation peaks.

The effect of dispersion is reduced with stronger coupling. For example, Fig. 9 shows the variation of ΔP with P, for 11-element guides with different κ. In each case, ΔP varies linearly with $P - P_C$, where $P_C = 6$ is the central element, and the slope is reduced towards zero by increasing $|\kappa|$. Simulations of longer guides with N up to 41 showed similar trends, and localization with $|\Delta P| < 0.5$ was possible merely provided $|\kappa|$ was large

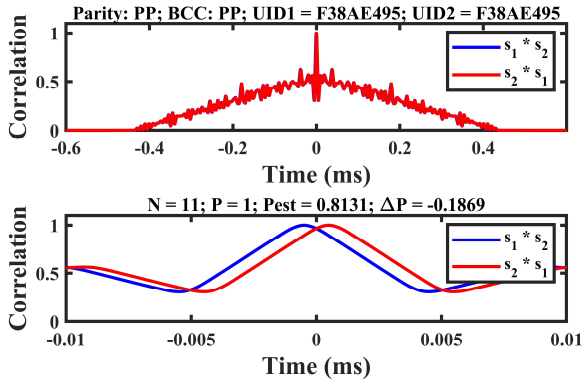

Fig. 8. Simulated noiseless cross-correlation plots over long and short timescales for $UID = F38FEA95$, assuming $N = 11$ and $P = 1$, assuming carrier and modulation amplitudes of 1.0 and 0.05.

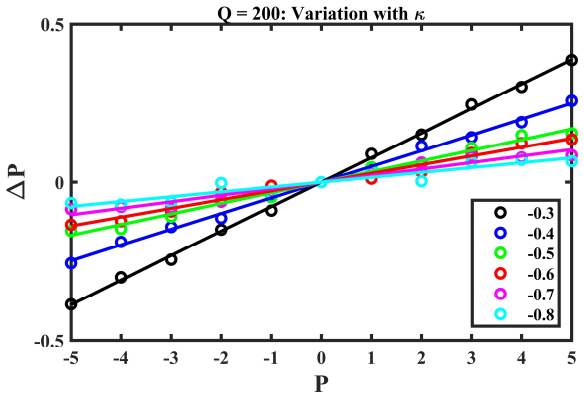

Fig. 9. Simulated variation of error ΔP with position P for noiseless 11-element guide with different coupling coefficient κ as given in the legend.

enough. If the tag is laterally offset, especially at non-zero range, load modulation signals may be induced in more than one element. It is simple to modify the model to include signals from a neighbor element. Their effect is to pull the estimated tag position toward the neighboring loop.

We have performed an initial investigation of the noise models in Fig. 2, using data from multiple simulations with the tag at position 1. In each case, noise defined by a standard deviation σ was added in the frequency domain before filtering. In Model 1, noise has a white spectrum; Model 2 noise is band-limited by the MI waveguide, and Model 3 noise is both band-limited and modulated by resonances. For Model 1, a single value of P_{est} close to unity was obtained for $\sigma = 0$ as described above. As σ rose, the probability density function (pdf) broadened into a Gaussian distribution. For Model 3, the pdf again broadened as σ increased. However, due to the correlated nature of the noise, the mean gradually shifted to the center of the array. Intermediate behavior was observed for Model 2, with the mean shifting more slowly towards the center.

V. Experimental Verification

In this section, we present an experimental verification of tag localization using a demonstration magneto-inductive antenna and a custom HF RFID transceiver.

Experiments were carried out using an 11-element MI antenna with an overall length just below $1.8m$. The number of

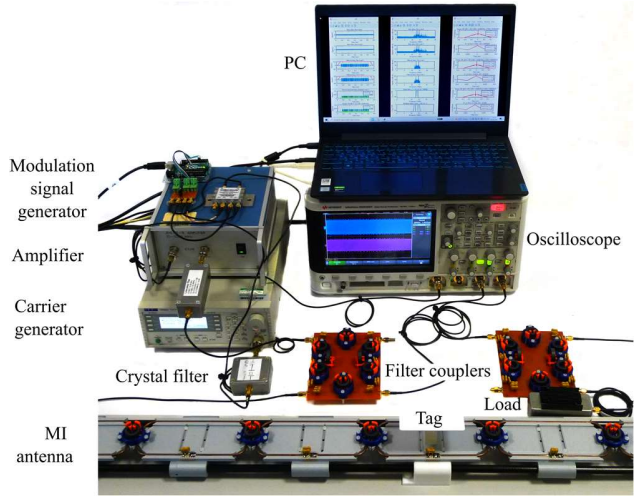

Fig. 10. HF RFID location detection system in operation with processed results displayed on PC screen and tag UID responses shown on oscilloscope.

elements was large enough to demonstrate operation, while use of an odd number provided a midpoint element with zero time of flight difference. Each resonant element was constructed from 1/8" outer diameter copper pipe, bent to shape and held in a planar arrangement using 3D-printed mounts fabricated using polylactic acid with relative a permittivity of approximately 2.5 [48]. Each element measured $W = 15\,cm$ x $H = 6\,cm$, and adjacent elements were spaced apart by $\sim 1.3\,cm$. This arrangement minimised coupling by free-space fields, reducing the likelihood of a tag being detected simultaneously by two elements. Nearest neighbor magnetic coupling was achieved using transformers based on low-loss ferrite toroidal elements (5967000601, Fair-Rite Products Corp.), wound so that $M < 0$. Coupling was mechanically adjustable over the range $-0.3 \leq \kappa \leq -0.6$ by using a rapid prototyped mechanism to alter the relative position of the two coil windings. Fig. 10 shows the complete system in operation with the tag placed at element 6 at 3cm separation. A short section of waveguide is seen at the bottom.

Tuning and matching were carried out using an electronic network analyzer (Agilent E5061B). The inductance was $L = 2.45\mu H$, and resonance was achieved at 13.56 MHz with a quality factor of $Q = 180$ using mica capacitors with $C = 56\,pF$. The coupling coefficient was adjusted to give a mid-band characteristic impedance of $Z_{0M} = 50\,\Omega$, which required $\kappa = -0.48$. To minimize unwanted reflections due to antenna imperfections, resonators were individually tuned to 13.56 MHz self-resonant frequency using varicaps, and mutual inductance was kept uniform through pair-wise tuning of coupling coefficients between elements. The upper diagram in Fig. 11 compares the theoretical dispersion characteristic from (2) (dotted line) with the measured resonant frequencies of an un-loaded 9-element guide (points), which lie at $ka = \nu\pi/10$, where $\nu = -9 \ldots -1$; agreement is excellent.

The lower diagram compares the theoretical frequency dependence of S-parameters for an 11-element guide obtained by solving the circuit equations (dotted line) with the experimental measurement (full line). The results show good

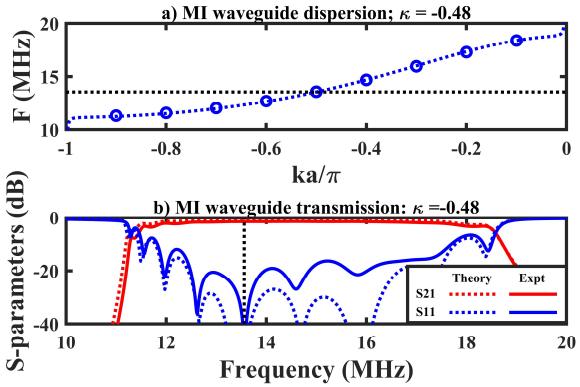

Fig. 11. a) Comparison of the theoretical dispersion characteristic with the experimental measurement of the resonances of a 9-element MI waveguide; b) Comparison of the theoretical variation of S-parameters with frequency with experimental measurement of an 11-element MI waveguide.

matching and low-loss propagation between $\sim 11MHz$ and $\sim 18.5MHz$ with a minimum loss of $1.5dB$, $\sim 0.5dB$ below the theory estimate.

A transceiver was constructed with the functionality of Fig. 1. Interrogation codes compliant with ISO/IEC 14443 Type A were generated using a personal computer and passed via a unique serial bus (USB) to a microcontroller (Arduino Uno) acting as a function generator. Output from the microcontroller was used to modulate a carrier at 13.56 MHz derived from a signal generator (TTi TGR6000) via an RF analogue switch (Minicircuits ZFSWHA-1-20+) to generate ASK at 106 kB/s. A quartz crystal filter was used to denoise the carrier. Signal strength was increased to a maximum 1 W using a power amplifier (Minicircuits ZHL-2-8), and a low-pass filter with a cutoff at 20 MHz was used to suppress harmonics. Signals were transferred into and out of the MI waveguide using lumped element filter couplers [49]. Detection of OOK tag responses was carried out using a digital storage oscilloscope (Keysight InfiniiVision DSOX3024T) sampling at 1.25 Gsa/sec, which acted as a signal acquisition buffer. Digitized signals were passed back to the PC via USB. Matlab-based filtering was used to suppress carrier and noise, and a Tukey window was again used to remove artifacts at window edges. UIDs were recovered by rectification, filtering and correlation with Manchester transition templates, and tag positions were estimated by correlation as described in Section 5.

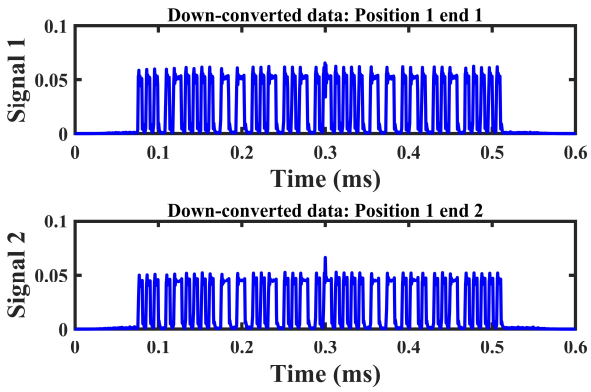

Fig. 12. Experimental measurement of down-converted signals obtained using the 11-element waveguide, for $UID = F38FEA95$ and $P = 1$.

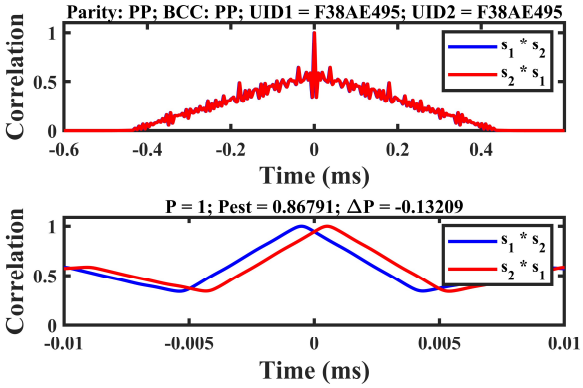

Fig. 13. Experimental cross-correlation signals over long (upper diagram) and short (lower) timescales obtained for $UID = F38FEA95$ and $P = 1$.

Experiments were carried out using 1k Mifare Classic RFID tags measuring $85mm\ x\ 54mm$ with a resonance at 14.5 MHz and an unloaded Q-factor of ~ 30, with the card placed at the center of each loop. The earlier Fig. 10c shows typical traces for $UID = F38FEA95$ during signal acquisition, highlighting the weak signals generated by load modulation. Despite this, tag responses were recovered easily. Fig. 12 shows recovered response envelopes with the tag at position $P = 1$ at $1W$ RF power. Signal 2 has slightly lower amplitude, due to the larger numbers of elements traversed.

Fig. 13 demonstrates successful parity and BCC checks and correct UID recovery from each channel. Cross-correlations plotted on long and short timescales indicate accurate localization with small position error (here, $\Delta P \approx -0.13$). Rounding of the correlation peaks is insignificant, and substantial agreement with Fig. 8 validates both the theoretical model and the general approach of timing by cross-correlation of UID responses.

As expected, the time delay between the two signals increased linearly with distance from the array center, with a peak delay of $\sim 1\mu s$. Fig. 14 shows the experimental variation of ΔP with P, obtained at zero range and different RF powers between $0.05W$ and $1W$. In each case, the tag UID was recovered correctly, and position was estimated with $|\Delta P| < 0.5$. At higher powers, the slope of the error variation is in good agreement with results in Fig. 9 for $\kappa = -0.5$; however, the slope reduced slightly as the RF power and SNR reduced.

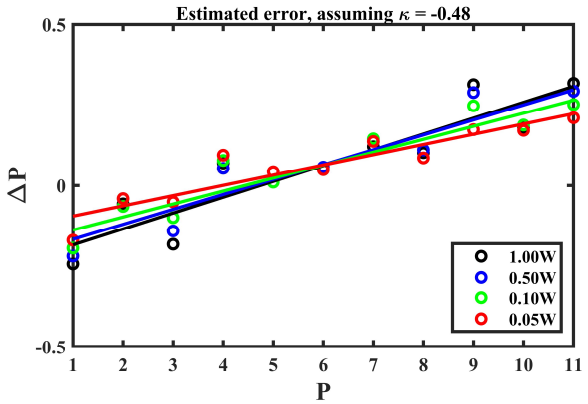

Fig. 14. Experimental variation of error ΔP with position P obtained using the 11-element MI waveguide at different RF powers as in the legend.

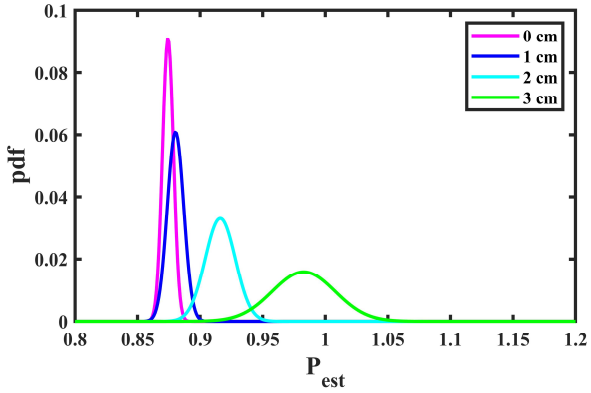

Fig. 15. Probability distributions for position obtained from 100 measurements of tag position with $P = 1$ for 1 W power at different ranges as in the legend.

Fig. 15 shows pdfs of estimated position obtained from 100 measurements with the tag at position 1, for $1W$ power and different transverse ranges. As the range increases and the SNR deteriorates, the distribution broadens and shifts towards the array center, implying that the most likely noise sources are Models 2 and 3 in Fig. 2. Tags were correctly localized up to 5 cm range, but errors fell outside acceptable limits at 6 cm, the conductor separation, when the UID was no longer recovered correctly. Results were similar for other Mifare tags, including best and worst cases with $UID = 010D354A$ and $UID = FFFFFFFF$ identified earlier. Localization of small fob-type tags was possible, but only for zero range at $1W$ RF power. Similar results were obtained by cross-correlation of reconstructed UID templates. Although correlation peaks were sharper, no convincing improvement in the mean or standard distribution of the estimated position was obtained.

VI. Discussion and Future Work

Experiments have shown that accurate location can be achieved at transverse ranges up to 6 cm at 1 W input power, matching the horizontal conductor separation of the resonator inductors. Larger separations resulted in insufficiently strong magnetic fields for interrogation. The tag footprint must lie within a single element to prevent coupling to neighboring loops; otherwise, two elements can be loaded simultaneously, creating two sets of reflected and transmitted sidebands. Localization accuracy is then degraded, and the tag position can only be determined to the nearest element. Positioning within a single element did not affect performance.

While highly effective at tag location, the current system has several limitations: the travelling wave antenna is rigid, maximum number of resonators is limited by group velocity dispersion, and location of multiple tags is not supported. Future work would involve the design of flexible waveguides based on loaded transmission lines with reduced group delay dispersion over HF RFID interrogation frequencies. The location method can be extended to multiple tags by sequentially interrogating UIDs. Investigation of architectures beyond the one-dimensional case is also of interest. Additionally, algorithms for location of tags loading pairs of elements simultaneously could be found, allowing spatially continuous detection regions along the antenna axis as in [43].

VII. Conclusion

A new method of one-dimensional HF RFID tag localization based on time-of-flight measurement of tag responses in a magneto-inductive travelling wave antenna has been proposed and demonstrated. The autocorrelations of ISO/IEC 14443 Type A UID responses have been investigated. A correlation detection scheme has been proposed, and simulations using a transfer function model with practical parameters have shown that flight times may be estimated by correlation of responses from either end of the antenna, provided the magnetic coupling coefficient is sufficiently high. TOF difference may be converted into distance-of-flight difference and thence to tag position using the MI wave group velocity, allowing localization to be combined with identification despite uncertainty in either the exact nature or the timing of the tag signal. Theoretical predictions have been confirmed experimentally using an 11-element model waveguide with small loop dimensions, and tag positions have been estimated accurately at transverse ranges up to the tag reading limit using RF power levels below $1W$.

There is potential to increase overall capture volume by scaling to larger loops and longer waveguides. Other waveguide formats such as lumped element $L-C$ transmission lines or $L-C$ resonators linked to continuous transmission lines could also be used, merely provided they combine external field regions suitable for tag powering and communication with low group velocity. Flexible printed antennas would reduce weight and bulk, improve consistency of resonant frequency and coupling and allow more general layouts. Meander waveguide layouts would enable quasi 2D tracking, while arrays might enable full 2D tracking based on the propagation of cylindrical waves. Such systems would enable asset or personnel tracking over much greater longitudinal distances than those currently used in HF RFID, without the need for large numbers of distributed transceivers. Alternative applications include the location of mobile devices for recharging purposes.

References

[1] R. Want, "An introduction to RFID technology," in *IEEE Pervasive Comput.*, vol. 5, no. 1, pp. 25-33, Jan.-Mar. 2006, doi: 10.1109/MPRV.2006.2.

[2] K. Finkenzeller, *RFID Handbook: Fundamentals and applications in contactless smart cards, radio-frequency identification and near-field communication,* 3rd ed., Chichester, UK: Wiley, June 2010.

[3] K. Curran, "Near field communication," *Int. J. Electr. Comp. Engng*. vol. 2, no. 3, pp. 371-382, June, 2012, doi: 10.11591/ijece.v2i3.234.

[4] *Cards and security devices for personal identification—contactless proximity objects*, ISO/IEC 14443, 2018.

[5] W. Aerts, E. De Mulder, B. Preneel, G. A. E. Vandenbosch and I. Verbauwhede, "Dependence of RFID Reader Antenna Design on Read Out Distance," in *IEEE Trans. Antennas and Propag.*, vol. 56, no. 12, pp. 3829-3837, Dec. 2008, doi: 10.1109/TAP.2008.2007378.

[6] B.Y. Tsirline, "Spatially selective antenna for very close proximity HF RFID applications," *High Freq. Electron.*, February Issue, pp. 18-28 (Part 1); March Issue, pp. 16-26 (Part 2), Mar. 2007.

[7] H. Hirayama, Y. Satake, N. Kikuma and K. Sakakibara, "Improvement of null zone avoidance capability for HF-band RFID using diversity combining of loop antennas," in *2009 3rd Eur. Conf. Antennas Propag.*, 2009, pp. 1594-1597.

[8] M. Y. Ahmad and A. S. Mohan, "Novel bridge-loop reader for positioning with HF RFID under sparse tag grid," in *IEEE Trans. Ind. Electron.*, vol. 61, no. 1, pp. 555-566, Jan. 2014, doi: 10.1109/TIE.2013.2245617.

[9] M. Benamara *et al*., "A Twisted Loop Antenna to enhance HF RFID detection for different tag positioning," in *2016 10th Eur. Conf. Antennas Propag.*, 2016, pp. 1-5, doi: 10.1109/EuCAP.2016.7481810.

[10] A. Boryssenko and E. Boryssenko, "Array antenna design for HF RFID smart cabinet," in *Proc. IEEE Conf. on Microw. Commun. Antennas Syst*., Tel Aviv, Israel, Nov. 7-9, 2011, doi: 10.1109/COMCAS.2011.6105875.

[11] Y. Mehlman, P. Kumar, M. Ozatay, S. Wagner, J.C. Sturn and N. Verma, "Large-area electronics HF RFID reader array for object-detecting smart surfaces," *IEEE Solid-State Circuits Lett*. vol. 1, no. 8, pp. 182-185, Aug. 2018, doi: 10.1109/LSSC.2019.2902063.

[12] I. Ehrenberg, C. Floerkemeier and S. Sarma, "Inventory management with an RFID-equipped mobile robot," in *Proc. IEEE Int. Conf. Automat. Sci. Engng*., Scottsdale, AZ, Sept. 22-25, 2007, pp. 1020-1026, doi: 10.1109/COASE.2007.4341838.

[13] L. Xu, J. Liu, X. Wang, H. Gong, Y. Wang and L. Chen, "HF RFID-based book localization via mobile scanning," in *Proc. IEEE Conf. on Sensing, Communication and Localization*, Como, Italy, June 22-25, 2020, doi: 10.1109/SECON48991.2020.9158442.

[14] S. Willis and S. Helal, "RFID information grid for blind navigation and wayfinding," in *Proc. 9th Int. Symp. Wearable Comput.,* Osaka, Japan, Oct. 18-21, 2005, doi: 10.1109/ISWC.2005.46.

[15] M. Baum, B. Niemann and L. Overmeyer, "Passive 13.56 MHz RFID transponders for vehicle navigation and lane guidance," in *Proc. 1st Int. EURASIP Workshop RFID Tech.*, Vienna, Austria, Sept. 24-25, pp. 83–86, 2007.

[16] K. Kodaka, H. Niwa, Y. Sakamoto, M. Otake, Y. Kanemori and S. Sugano, "Pose estimation of a mobile robot on a lattice of RFID tags," in *Proc. IEEE/RSJ Int. Conf. Intell. Robots Syst.*, Nice, France, Sept. 22-26, 2008, pp. 1385-1390, doi: 10.1109/IROS.2008.4651176.

[17] P. Yang, W. Wu, M. Moniri and C.C. Chibelushi, "Efficient object localization using sparsely distributed passive RFID tags*," IEEE Trans. Indust. Elect*., vol. 60, no. 12, pp. 5914-5924, Nov. 2013, doi: 10.1109/TIE.2012.2230596.

[18] J. Mi and Y. Takahashi, "Design of an HF-band RFID system with multiple readers and passive tags for indoor mobile robot self-localization," *Sensors*, vol. 16, no. 8, pp. 1200, July 2016, doi: 10.3390/s16081200.

[19] A.A.N. Shirehjini and S. Shirmohammadi, "Improving accuracy and robustness in HF-RFID-based indoor positioning with Kalman filtering and Tukey smoothing," *IEEE Trans. Instrum. Meas*., vol. 69, no. 11, pp. 9190-9202, May 2020, doi: 10.1109/TIM.2020.2995281

[20] L.M. Ni, Y. Liu, Y.C. Lau and A.P. Patil, "LANDMARC: indoor location sensing using active RFID," in *Proc. 1st IEEE Conf. on Pervasive Comput. Commun.*, Fort Worth, TX, Mar. 23-26, 2003, pp. 407–415, doi: 10.1109/PERCOM.2003.1192765

[21] Y. Zhang, M.G. Amin and S. Kaushnik, "Localization and tracking of passive RFID tags based on direction estimation," Int. J. Antennas Propag. vol. 2007, pp. 17426, December, 2007, doi: 10.1155/2007/17426

[22] Y. Park, J.W. Lee and S. Kim, "Improving position estimation on RFID tag floor localization using RFID reader transmission power control," in *Proc. IEEE Int. Conf. Robotics Bioinformatics*, Bangkok, Thailand, Feb. 21-26, 2009, pp. 1716-1721, doi: 10.1109/ROBIO.2009.4913260.

[23] C. Hekimian-Williams, B. Grant, X. Liu, Z. Zhang and P. Kumar, "Accurate localization of RFID tags using phase difference," in *Proc. IEEE Int. Conf. RFID, Orlando*, FLA, Apr. 14-16, 2010, pp. 89-96, doi: 10.1109/RFID.2010.5467268.

[24] J. Wang and D. Katabi, "Dude, where's my card? RFID positioning that works with multipath and non-line of sight," in *Proc. SIGCOMM'13*, Hong Kong, China, Aug. 12-16, 2013, pp. 51-62, doi: 10.1145/2486001.2486029.

[25] M. Scherhäufl, M. Pichler and A. Stelzer, "UHF RFID localization based on phase evaluation of passive tag arrays," *IEEE Trans. Instrum. Meas.,* vol. 64, no. 4, pp. 913-922, Apr. 2015, doi: 10.1109/TIM.2014.2363578

[26] H. Wu, B. Tao, Z. Gong, Z. Yin and H. Ding, "A fast UHF RFID localization method using unwrapped phase-position model," *IEEE Trans. Automation Sci. Engng*., vol. 16, no. 4, pp. 1698-1707, Oct. 2019, doi: 10.1109/TASE.2019.2895104.

[27] A.R. Chatzistefanou, A. Tzitsis, S. Megalou et al., "Trajectory tracking of UHF RFID tags, exploiting phase measurements collected from fixed antennas," *IEEE J. RFID*, vol. 5, no. 2, pp. 191-206, June 2021, doi: 10.1109/JRFID.2021.3053101.

[28] L.M. Li and D. Zhang, "RFID-based localization and tracking technologies*," IEEE Wireless Comms.,* vol. 18, no. 2, pp. 45-51, Apr. 2011, doi: 10.1109/MWC.2011.5751295.

[29] H. Liu, H. Darabi, P. Banerjee and J. Liu, "Survey of wireless indoor positioning techniques and systems," *IEEE Trans. Systems, Man and Cybernetics Part C*, vol. 37, no. 6, pp. 1067-1080, 2007, doi: 10.1109/TSMCC.2007.905750.

[30] C. Li, L. Mo and D. Zhang, "Review on UHF RFID localization methods," *IEEE J. RFID*, vol. 3, no. 4, pp. 205-215, June 2019, doi: 10.1109/JRFID.2019.2924346.

[31] E. Shamonina, V.A. Kalinin, K.H. Ringhofer and L. Solymar, "Magnetoinductive waveguide," *Electron. Lett*., vol. 38, no. 8, pp. 371-373, Apr. 2002, doi: 10.1049/el:20020258.

[32] M.C.K. Wiltshire, E. Shamonina., I.R. Young and L. Solymar, "Dispersion characteristics of magneto-inductive waves: comparison between theory and experiment," *Elect. Lett.,* vol. 39, no. 2, pp. 215-217, Jan. 2003: doi 10.1049/el:20030138.

[33] E. Shamonina and L. Solymar, "Magneto-inductive waves supported by metamaterial elements: components for a one-dimensional waveguide," *J. Phys. D. Appl. Phys.*, vol. 37, no. 3, pp. 362-367, Jan. 2004, doi: 10.1088/0022-3727/37/3/008.

[34] RR.A. Syms, I.R. Young, L. Solymar and T. Floume, "Thin-film magneto-inductive cables," *J. Phys. D. Appl. Phys*., vol. 43, no. 5, pp. 055102, Jan. 2010, doi: 10.1088/0022-3727/43/5/055102.

[35] R.R.A. Syms, L. Solymar and I.R. Young, "Broad-band coupling transducers for magneto-inductive cable," *J. Phys. D. Appl. Phys.,* vol. 43, no. 28, pp. 285003, June 2010, doi: 10.1088/0022-3727/43/28/285003.

[36] C.J. Stevens, C.W.T. Chan, K. Stamatis and D.J. Edwards, "Magnetic metamaterials as 1-D data transfer channels: an application for magneto-inductive waves," *IEEE Trans. Micr. Theory Tech.*, vol. 58, no. 5, pp. 1248-1256, Apr. 2010, doi: 10.1109/TMTT.2010.2045562.

[37] Z. Sun and I.F. Akyildiz, "Magnetic induction communications for wireless underground sensor networks," *IEEE Trans. Antennas Propag*., vol. 58, no. 7, pp. 2426-2435, July, 2010, doi: 10.1109/TAP.2010.2048858.

[38] B. Gulbahar and O.B. Akan, "A communication theoretical modeling and analysis of underwater magneto-inductive wireless channels," *IEEE Trans. Wireless Commun.,* Vol. 11, no. 9, pp. 3326-3334, Sept., 2012, doi: 10.1109/TWC.2012.070912.111943.

[39] T. Floume, "Magneto-inductive conductivity sensor" *Metamaterials,* vol. 5, no. 4, pp. 206-217, Dec. 2011, doi: 10.1016/j.metmat.2011.08.003.

[40] J. Yan, C.J. Stevens and E. Shamonina, "A metamaterial position sensor based on magneto-inductive waves," *IEEE Open J. Antennas Propag*., vol. 2, pp. 259-268, Feb. 2021, doi: 10.1109/OJAP.2021.3057135.

[41] I. Khromova, C.J. Stevens and E. Chatziantoniou, "Load localisation," WO 2020/128520, Dec. 20, 2019.

[42] T. Trivedi, Y. Chen, I.A.D. Williamson, P. Pasupathy and D.P. Neikirk, "Group velocity estimation and defect localization in magneto-inductive waveguides," *IEEE Trans. Micr. Theory. Tech*., vol. 69, no. 4, pp. 2072-2077, Apr. 2021, doi: 10.1109/TMTT.2021.3055350.

[43] R.R.A. Syms, O. Sydoruk and M.C.K. Wiltshire, "Magneto-inductive HF RFID system," *IEEE J. RFID,* vol. 5, no. 2, pp. 148-153, June, 2021, doi: 10.1109/JRFID.2020.3042719.

[44] T. Kailath, "Correlation detection of signals perturbed by a random channel," *IRE Trans. Inform. Theory*, vol. 6, no. 3, pp. 361-366, June, 1960, doi: 10.1109/TIT.1960.1057563.

[45] L.A. Pflug, "Prefiltering for improved correlation detection of bandlimited signals," *J. Acoust. Soc. Amer*., vol. 95, no. 3, pp. 1459-1473, Mar 1994, doi: 10.1121/1.408587.

[46] E.J. Cummins, S. Jauregui and W.R. Vincent, "Time- and frequency domain characteristics of man-made radio noise affecting HF-communications sites," *IEEE Trans. Electromagn. Compat*., vol. EMC-21, no. 3, pp. 182-189, Aug. 1979, doi: 10.1109/TEMC.1979.303730.

[47] T.W.H. Fockens, A.P.M. Zwamborn and F. Leferink, "Measurement methodology and results of measurements of the man-made noise floor on HF in the Netherlands," *IEEE Trans. Electromagn. Compat*. vol. 61 no. 2, pp. 337-343, Apr. 2019, doi: 10.1109/TEMC.2018.2830512.

[48] C. Dichtl, P. Sippel and S. Krohns, "Dielectric Properties of 3D Printed Polylactic Acid," *Advances in Materials Science and Engineering*, 2017 doi: 10.1155/2017/6913835.

[49] A. Voronov, R. R. A. Syms, and O. Sydoruk, "High-Performance Magnetoinductive Directional Filters," *Electronics*, vol. 11, no. 6, p. 845, Mar. 2022, doi: 10.3390/electronics11060845.